Harmonic calculations and measurements of the irreversibility field using a vibrating sample magnetometer

Ian J. Daniel and Damian P. Hampshire
Department of Physics, Superconductivity Group, University of Durham, South Road, Durham DH1 3LE, England
(Received 17 September 1999)

The effect of the field inhomogeneity of the magnet on a vibrating sample magnetometer (VSM) measurement of a superconductor is calculated using Bean's model and Mallinson's principle of reciprocity. When the sample is centered in both the magnetic field and the VSM pick-up coils, the hysteretic signal obtained in a VSM measurement, associated with the critical current density (J_C), is reduced to zero when the effective ac field caused by the sample movement penetrates the entire sample and not, as is commonly assumed, when the critical current density becomes zero. Under these conditions, an apparent phase transition is observed where the magnitude of the hysteresis drops to zero over a small field range. This apparent transition is solely an artifact of the measurement and cannot correctly be compared to theoretical calculations of the irreversibility field (B_{IRR}), which is the phase boundary at which J_C is zero. Furthermore, the apparent reversible magnetization signal in high fields includes two contributions. In addition to the usual diamagnetic contribution from the thermodynamic reversible magnetization of the superconductor, there is a reversible paramagnetic contribution from the nonzero J_C. Hence values of the Ginzburg-Landau parameter (κ) cannot be reliably obtained from standard reversible magnetization measurements using a VSM unless it is confirmed that J_C is zero. Harmonic measurements using a VSM are reported. They confirm the results of the calculations. By applying a large field gradient, the hysteresis in the magnetization signal at the drive frequency of the VSM is found to drop to zero more than 3 T below B_{IRR}. We propose methods to improve measurements of B_{IRR} and κ. The implications of results presented for superconducting quantum interference device measurements are also briefly discussed.

I. INTRODUCTION

Although zero resistance is probably the most widely known property of superconductors, there is little doubt that their magnetic properties have provided most insight into the underlying science of these materials. The irreversibility field B_{IRR}, which is by definition the field at which J_C drops to zero has been the focus of a great deal of theoretical and experimental work.[1–4] The earliest HTS (high temperature superconductors) showed an irreversibility field well below the upper critical field (B_{C2}), consistent with the short coherence length.[5] Technological interest in these materials utilizes B_{IRR} to provide a practical magnetic field limit for the material's use in superconducting applications so that increasing B_{IRR}, improves a material's utility. The connection between B_{IRR}, the fundamental superconducting properties and the materials' fabrication is still not fully understood. Above B_{IRR}, reversible magnetization data on low-[6] and high-temperature superconductors[7–9] can be equated to the thermodynamic reversible magnetization obtained from Ginzburg-Landau theory and the Ginzburg-Landau parameter (κ) derived.[10,11] The Ginzburg Landau parameter plays a critical role in the theoretical description of the fundamental high-field properties of superconductors. This article provides detailed calculations and measurements that facilitate correct interpretation and improvement of very high sensitivity magnetic measurements on superconductors using a Vibrating Sample Magnetometer[12] (VSM). Harmonic VSM measurements are reported and methods proposed to obtain more reliable values of B_{IRR} and κ.

Vibrating sample magnetometer and superconducting quantum interference device (SQUID) measurements are the most widespread techniques for measuring both the hysteretic and reversible magnetic response of Type-II high-field superconducting materials. The SQUID systems are most common because of their excellent sensitivity. However for measurements in fields above ~10 T, screening of the SQUID becomes problematic and the VSM is favored. It has long been appreciated that the field inhomogeneity of the magnet distorts the signal obtained in a SQUID measurement when the self-field of the sample is comparable to the change in the applied field the sample experiences as it moves between the SQUID pick-up coils.[13,14] This is particularly so for single crystals.[15] Nevertheless because the SQUID measurement captures data that describes the *total* flux produced by the sample, careful analysis of the voltage output can in principle still extract the critical current even if the applied field is inhomogeneous.[16,17] The effect of field inhomogeneity in a standard VSM measurement is fundamentally different to that of the SQUID. In a VSM measurement, the signal is measured only at the drive frequency of the oscillation to improve the signal-to-noise ratio. Therefore signal that occurs at harmonic frequencies is automatically lost. This loss of information profoundly affects the origin of the field at which the magnetic hysteresis drops to zero (B^*_{IRR}) and measurements of the Ginzburg-Landau parameter derived from reversible magnetization data in fields above B^*_{IRR}. In particular B^*_{IRR} data obtained exclusively at the drive frequency of the oscillation of the VSM may not be directly equated to B_{IRR}. In this article, data are reported at harmonic frequencies of the drive frequency, which maintain good signal-to-noise and capture the entire signal.

Although much work has been completed on optimizing the geometry of the pick-up coils for a VSM,[18] the effect of the inhomogeneity of the magnetic field in a VSM system has not been addressed in detail. This article shows that it can play a critical role in determining B^*_{IRR} and the reversible magnetization above B^*_{IRR}. B^*_{IRR} is the field at which the effective ac field penetrates the entire sample and not, as is commonly assumed, when the critical current density becomes zero (i.e., $B^*_{\mathrm{IRR}} \neq B_{\mathrm{IRR}}$).[19,20] At fields close to B^*_{IRR} the hysteresis cannot be equated to J_C. Indeed the rapid reduction in the hysteresis at B^*_{IRR} that is often interpreted as a phase transition is in fact an artifact of the measurement. When the sample is centered in both the pick-up coils and the applied field, above B^*_{IRR} the measured reversible magnetization has two components. In addition to the thermodynamic reversible diamagnetic magnetization, there is an additional reversible paramagnetic contribution from the nonzero J_C. Hence although the reversible magnetization properties of a superconductor probably provide the most effective way to parametrize the material within the framework of Ginzburg-Landau theory, unless it is confirmed that J_C is zero, the fundamental parameters derived from standard reversible magnetization data are not correct.

The next section provides detailed calculations of the response of a Type-II superconductor within a standard VSM measurement. It is assumed that the material has bulk pinning described by Bean's model[19] so the calculations can apply to both low- and high-temperature superconductors. Mallinson's principle of reciprocity[21] is used to describe the instantaneous voltages produced during a VSM measurement. Harmonic measurements and analysis are used. These are both well-established tools for investigating the underlying processes that produce the magnetic response of materials. In Campbell's flux penetration technique,[22] harmonic measurements have been used to distinguish bulk pinning from surface pinning.[23,24] In susceptibility measurements, the harmonic response has been used to measure the field dependence of J_C in low fields[25,26] and granularity.[27] This article reports harmonic data using a VSM. They are used to determine whether or not J_C is zero above B^*_{IRR} and confirm the results of the calculations. Then the implications for our general understanding of magnetic measurements that characterize the magnetic phase diagram of superconductors and a method to improve measurements of B_{IRR} and κ are discussed. Finally our conclusions are summarized.

II. CALCULATIONS

In this section, detailed calculation of the voltages produced during a VSM measurements are provided. The effects of a magnetic field gradient and the sample not being perfectly centered in the pick-up coils are included. The calculations demonstrate the important features of VSM measurements in real rather than ideal conditions. Before detailed calculations, consider the following estimate of the magnitude of the effects addressed in this article. In a typical commercial VSM the throw distance is $\sim$0.5 mm and the field homogeneity is $\sim 10^{-4}$ over a 1 cm diameter sphere. In general the field is more uniform in the central region at the peak so a reasonable value for the variation in field over $\sim$0.5 mm at 10 T is $\sim$5 μT. Although this is a relatively small field variation, it is approximately the same size as the self-field produced by a 1 mm^3 sample with a J_C of 4×10^3 Am^{-2}. For a 40 μm thin film, a critical current density of $\sim 10^5$ Am^{-2} produces 5 μT. Hence at relatively high critical current densities, the magnitude of the ac field the sample experiences during a VSM measurement, that is produced by the inhomogeneity of the magnet, is equal to the self-field of the sample. The calculations below confirm that when this equality occurs, the history of the sample is completely lost and Bean's model cannot be applied assuming the applied field is homogenous. The hysteresis in the magnetic moment found in a VSM measurement drops to zero producing an apparent phase transition that is entirely an artifact of the measurement.

A. Magnetic fields and mallinson fields

In Fig. 1(a), the standard idealized configuration of magnet and pick-up coils is shown for a VSM measurement. The magnetic sample oscillates up and down in the z direction, which generates a voltage across the pick-up coils. The sample is at the center (and peak) of the magnetic field and is centered between two oppositely wound pick-up coils. The analysis is simplified by assuming the magnetic field (B_{Mag}) points in the z direction and has a roof profile as shown in Fig. 1(a). It is also assumed that the sample is centered radially and its oscillation is sinusoidal.

The instantaneous voltage generated across the pick-up coils by the sample can be calculated by applying Mallinson's principle of reciprocity. The principle states that the mutual flux linking two coils is independent of which coil carries the current. Hence the voltage produced by an elemental magnetic moment oscillating between the pick-up coils as shown in Fig. 1(b) is equivalent to the voltage across a coil of elemental area that replaces the magnetic moment if unit current passes through the pick-up coils. The dotted lines in Fig. 1(b) denote the Mallinson field generated by unit current in each pick-up coil and the solid line shown gives the net Mallinson field. The Mallinson field points in the z direction. If the elemental moment is not centered in the pick-up coils, the instantaneous Mallinson field it experiences while it oscillates is: $\beta_0 \cos(\omega t)+\beta_1$, where β_1 is the Mallinson field at the center of the oscillation, $2\beta_0$ is the peak-to-peak Mallinson field during the oscillation [as shown in Fig. 1(c)] and ω is the angular frequency of the oscillation. Hence the instantaneous magnetic flux (ϕ) linking the pickup coils in the VSM measurement is

$$\phi = G[\beta_0 \cos(\omega t) + \beta_1] m(t), \tag{1}$$

where $m(t)$ is the magnetic moment of the sample, G, β_0 and β_1 are determined by the geometry of the pickup coils. β_1 is also determined by how far the sample is off-set from the center of the pick-up coils. From Fig. 1(c), it can be seen that the ratio β_0/β_1 is the ratio of half the throw distance to the distance the elemental moment is offset from the center of the pick-up coils. The voltage induced in the pick-up coils is given by

$$V = -\frac{\partial \phi}{\partial t} = -\frac{\partial}{\partial t}\{G[\beta_0 \cos(\omega t) + \beta_1] m(t)\}. \tag{2}$$

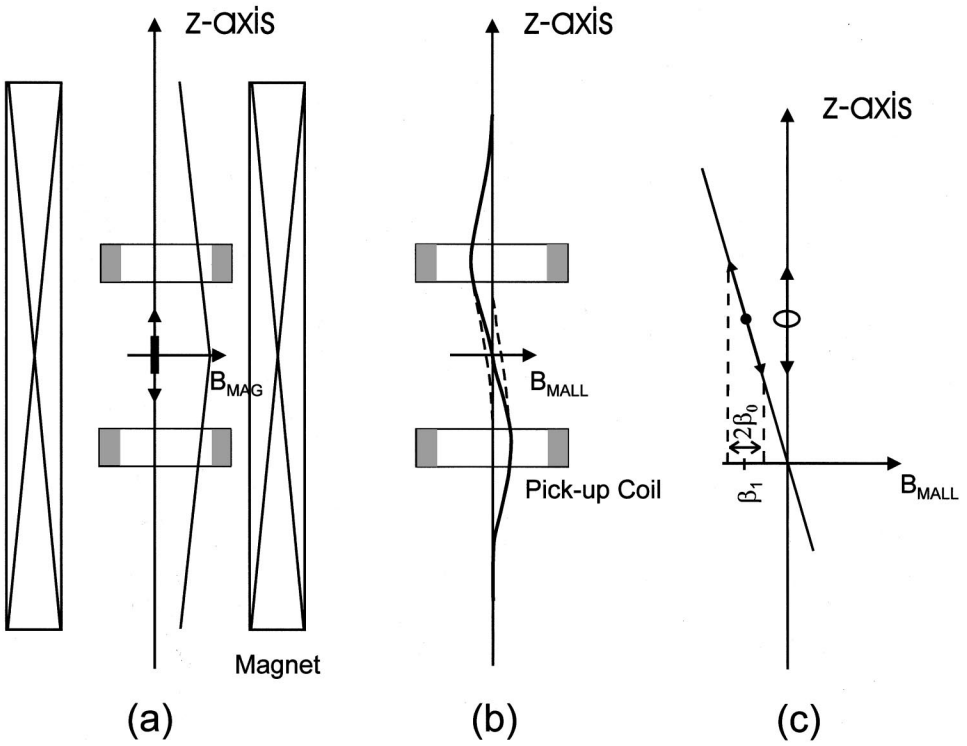

FIG. 1. The magnet, sample, and pick-up coil configurations used in the calculations. (a) Ideal configuration—the sample oscillates in the center of the pick-up coils and in the center of the applied field. The axes describe the magnitude of the applied field as a function of distance along the z axis. The applied field points along the positive z axis and has a roof profile. (b) The Mallinson field generated by unit current in the oppositely wound pick-up coils. The axes describe the magnitude of the Mallinson field as a function of distance along the z axis. The dotted lines denote the field generated by each coil separately and the solid line the net Mallinson field. The Mallinson field points along the z axis. (c) A schematic showing the Mallinson field experienced by an elemental magnetic moment that is oscillating off-centered in the pick-up coils.

In the idealized operation of a VSM, the magnetic moment is constant during the oscillation and the sample is perfectly centered in the pick-up coils ($\beta_1 = 0$). The geometry of the pick-up coils ensures that the gradient of the Mallinson field is constant over the throw distance. A pure sine wave voltage is observed at the drive frequency the magnitude of which is proportional to the magnetic moment of the sample.

B. The voltages produced by a sample oscillating in a uniform field gradient

This section first presents the voltages generated in a VSM measurement when the sample is centered in the pick-up coils but offset from the center of the applied field. Hence the sample is oscillating in a constant field gradient. Bean's model[28] is used to determine the instantaneous magnetic moment. Equation (2) is then used to calculate the voltages generated during the measurement.

The field profiles generated within the sample using Bean's critical state model for a superconducting cylinder of radius r_m and length l, moving in a constant field gradient during a VSM measurement are shown in Fig. 2. The field is applied along the axis of the cylinder. In low fields, the sample is not fully penetrated. In high fields, after a time t_γ, the ac field fully penetrates the sample. A parameter γ can be defined as the ratio between the peak value of the effective ac field and the sample self-field where

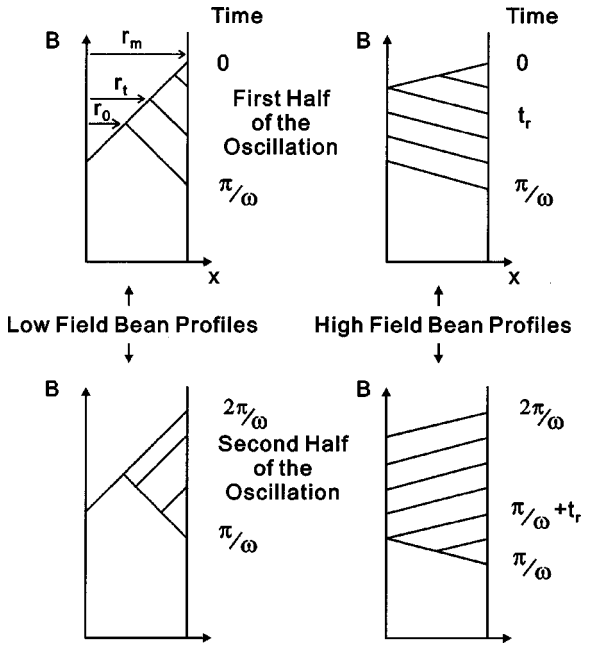

FIG. 2. Bean profiles for both the low- and high-field regimes. The radius of the sample is r_m. The distance from the center of the sample that the effective ac field penetrates is r_0. The turning point for the field profile is denoted r_t.

$$\gamma = \frac{B_{\mathrm{ac}}}{\mu_0 J_c r_m}. \tag{3}$$

In general $B_{\mathrm{ac}} = FB$ where F is a geometrical constant determined by the magnet and the throw distance of the VSM, and B is the applied peak field. In the calculations presented in this article, $F = 10^{-3}$. When the sample moves in a constant field gradient, $\gamma = 1$ separates the high-field regime from the low-field regime. It also characterizes when the history of the sample is lost and hence the condition for the applied field to be B^*_{IRR}. In low fields, from the Bean profiles in Fig. 2, the magnetic moment $[m(t)]$ is calculated by summing the screening currents throughout the volume of the sample:

$$m(t) = \Sigma IA = \int_0^{r_0} J_C \pi r^2 l dr \pm \int_{r_0}^{r_t} J_C \pi r^2 l dr \mp \int_{r_t}^{r_m} J_C \pi r^2 l dr$$

$$= \frac{J_C \pi l}{3}(r_0^3 \pm 2r_t^3 \mp r_m^3 \mp r_0^3), \tag{4}$$

where the upper signs are for the first half of oscillation and the lower signs for the second half of the oscillation. From Fig. 2, Bean's critical state model implies $r_0 = r_m(1-\gamma)$ for $\gamma \leqslant 1$. In the low field case, $r_t = r_m[1-\gamma(1-\cos \omega t)/2]$. In the high-field case, $m(t)$ is calculated in the four time domains: $0 < t < t_r$, $t_r < t < \pi/\omega$, $\pi/\omega < t < \pi/\omega + t_r$, and $\pi/\omega + t_r < t < 2\pi/\omega$. Thereafter, the time dependence of the magnetic moment has been calculated as a function of γ (or equivalently B). The critical current density has arbitrarily been taken to follow the simple linear-field dependence of the form:[29]

$$J_C = \alpha(B_{C2} - B), \tag{5}$$

where α is $5 \times 10^5\ \mathrm{A m^{-2} T^{-1}}$, B is the applied dc field and B_{C2} is taken as 10 T. Clearly there is no irreversibility field below B_{C2} for this functional form of J_C. Other functional forms for the field dependence of J_C will be considered below to demonstrate the generality of the results obtained. In Fig. 3, the time dependence of the magnetic moment for different values of γ are shown. The calculations were completed using Maple V Release 4 taking $\beta_0 = 1, \beta_l = 0, \omega = 200\pi, l = 4 \times 10^{-3}$ m, $r_m = 10^{-3}$ m. At very low values of γ (c.f., $\gamma = 0$) the field gradient is small and the magnetic moment does not change during the oscillation. For $\gamma \geqslant 1$, the history of the magnetic moment is completely lost and the mean value of the magnetic moment during the oscillation drops to zero. Figure 4 shows the equivalent voltages generated using Eq. (2), and $G = 0.538$. These values give a signal of $5\ \mathrm{mV_{rms}}$ at the drive frequency when J_C is $5 \times 10^6\ \mathrm{A m^{-2}}$ in zero field The voltage has been Fourier analyzed into a Fourier series and calculated as a function of field as shown in Fig. 5. The sine terms are denoted the lossless voltages (or lossless magnetic moment) and the cosine terms are the loss voltages. The calculations show that when β_0 is nonzero, a voltage occurs at the fundamental frequency (1f) and at even multiples of the drive frequency (i.e., even harmonics: 2f, 4f, 6f,...). We have confirmed that the 1f lossless voltage alone, which is normally taken to be proportional to the value of J_C, changes sign when the history of the applied field is changed. Furthermore it falls to zero at $\gamma = 1$. When $\gamma = 1$, the effective ac field caused by the movement of the sample is equal to the self-field of the sample and penetrates the sample completely. The width of the hysteresis measured at 1f does not represent the true critical current density of the sample. Although J_C drops to zero at 10 T (i.e., B_{C2}), the 1f hysteretic signal drops to zero at a field below 4 T. Hence the size of the hysteresis drops by many orders of magnitude over a small field range, which can be easily misinterpreted as a phase transition. In Sec. IV, we utilize the absence of any contribution from the bulk pinning to the 1 f signal above B^*_{IRR} in this configuration in proposing an improved measurement technique. The harmonic voltages generated have also been calculated for when the sample is not perfectly centered in the pick-up coils (β_l has been taken as -2). The β_l term produces additional voltages at odd multiples of the drive frequency (i.e., odd harmonics: 1f, 3f, 5f,...) as shown in Fig. 6.

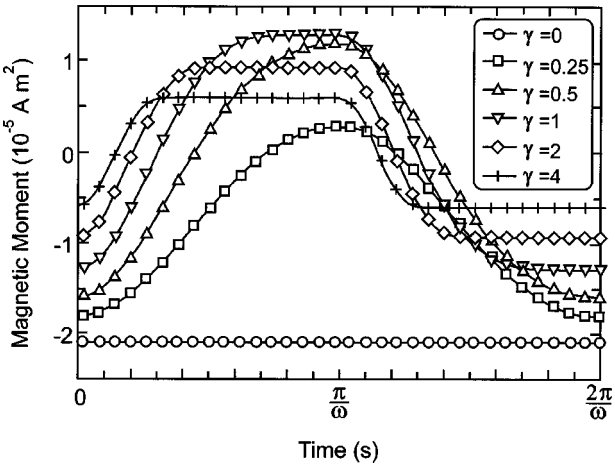

FIG. 3. Calculated values of the instantaneous magnetic moment of the sample for different values of ac field penetration. The ac field penetration is characterized by γ, where $\gamma = 10^{-3} B/\mu_0 J_C r_m$, $J_C = 5 \times 10^5 (B_{C2} - B)\ \mathrm{A m^{-2}}$, $B_{C2} = 10$ T, $l = 4 \times 10^{-3}$ m and $r_m = 10^{-3}$ m. When $\gamma = 1$, the sample is fully penetrated.

In Table I, a summary of the extensive calculations for

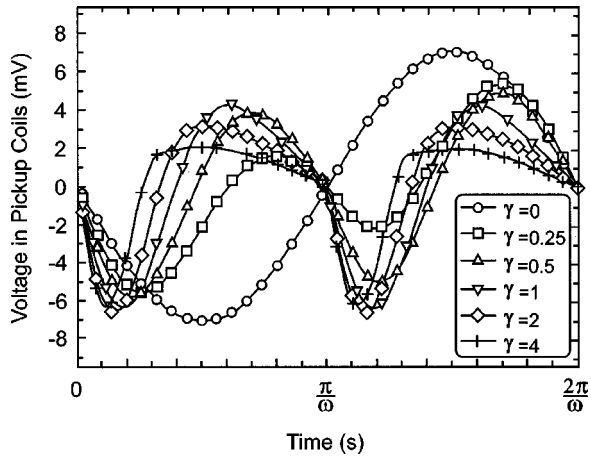

FIG. 4. The calculated voltage waveform across the pick-up coils for different values of ac field penetration. The ac field penetration is characterized by γ, where $\gamma = 10^{-3} B/\mu_0 J_C r_m$, $J_C = 5 \times 10^5 (B_{C2} - B)\ \mathrm{A m^{-2}}$, $B_{C2} = 10$ T, $l = 4 \times 10^3$ m and $r_m = 10^{-3}$ m. When $\gamma = 1$, the sample is fully penetrated.

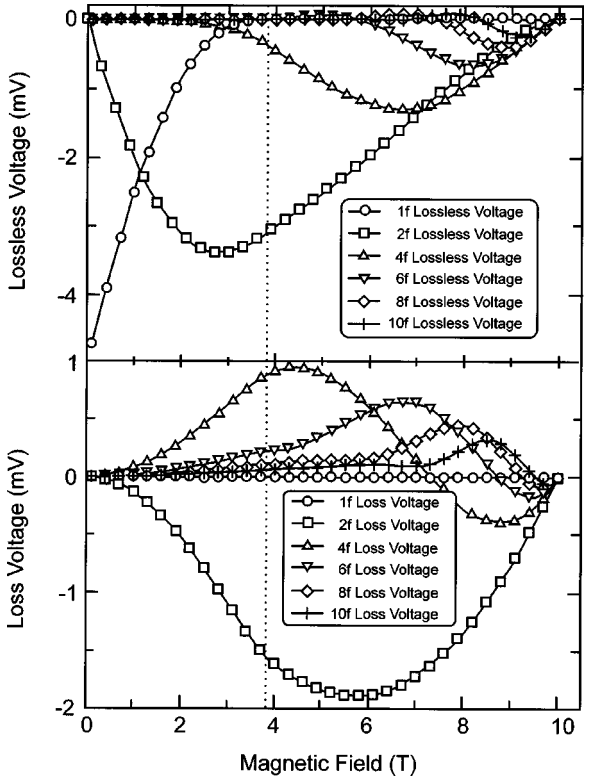

FIG. 5. Calculated harmonic voltages as a function of dc magnetic field for a sample in a uniform applied field gradient, centered in the pick-up coils. Upper panel—lossless voltages. All the odd harmonic voltages are zero except the fundamental frequency (1f) which alone changes sign (from diamagnetic shown when the dc field is increased) to paramagnetic when the dc field is decreased. All even harmonic voltages tend to zero at B_{C2}. Lower panel—loss voltages. All the odd harmonic voltages (including the fundamental that is shown) are zero. The dotted line indicates $\gamma=1$. The sample is characterized by $J_C=5\times10^5(B_{C2}-B)$ Am^{-2}, $B_{C2}=10$ T and $l=4\times10^{-3}$ m and $r_m=10^{-3}$ m.

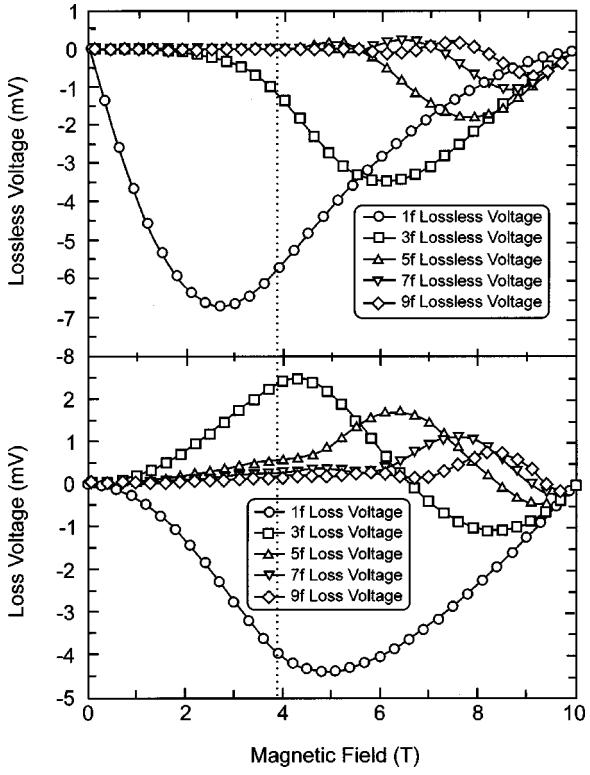

FIG. 6. Calculated additional harmonic voltages as a function of dc magnetic field due to the sample not centered in the pick-up coils (i.e., $\beta_1=-2$). Upper panel—lossless voltages. All the even harmonic voltages are zero. All odd harmonic voltages tend to zero at B_{C2}. Lower panel—loss voltages. All the even harmonic voltages are zero. The dotted line indicates $\gamma=1$. The sample is characterized by $J_C=5\times10^5(B_{C2}-B)$ Am^{-2}, $B_{C2}=10$ T and $l=4\times10^{-3}$ m and $r_m=10^{-3}$ m.

different configurations of the pick-up coils, the magnet, and the sample are presented. The first row of data describes the results shown in Fig. 5. At the fundamental frequency (1f), the lossless voltage is zero above B^*_{IRR}, whereas the even harmonic voltages are nonzero in fields up to B_{C2} (consistent with J_C only dropping to zero at B_{C2}). If the sample is offset in the pick-up coils, additional voltages are produced (second row of data, Table I), which are all (including 1f) nonzero up to B_{C2}. These additional reversible components can be either positive or negative (i.e., paramagnetic or diamagnetic) depending on whether the sample is above or below the center of the pick-up coils.

C. The voltages produced by a sample oscillating about the center of the dc field

Calculations have also been completed for a sample that oscillates symmetrically about the center of a roof magnetic field profile with a constant slope on either side. This configuration is considerably more complex than the previous ones but of most interest to experimentalists.

In Fig. 7, the oscillation of a sample about the field center is shown. Figure 7(a) shows how the applied field for five different points (i.e., A to E) varies with time. The parts of the sample above A and below E do not cross the center of the field. Their response follows that outlined in Sec. II B. In the central region, the applied field depends on the precise location within that region. Hence the parameter Z^* has been introduced, which defines the position of any element of the sample with respect to the center of the sample. Figure 7(b) shows that in general each element sees a large-field oscillation and a small-field oscillation. Figure 8 shows how the penetration of the sample in the positive central region (i.e., $Z^*>0$) develops as the applied field (and hence the size of the field oscillations) increases. Initially neither the small-field oscillation nor the large field oscillation fully penetrate the sample. When $\gamma=1$, there is the first penetration of the sample by the large-field oscillation at $Z^*=D/2$. In the regime $1<\gamma<2$, for $Z^*\geqslant D/\gamma-D/2$ the sample is only fully penetrated by the large-field oscillation. For $Z^*<D/\gamma-D/2$ the sample is not fully penetrated by either field oscillation. At $\gamma=2$, the large-field oscillation fully penetrates the sample throughout the positive central region and the small-field oscillation starts to penetrate the central region at $Z^*=0$. In the regime $\gamma>2$, for $Z\leqslant D(1-2/\gamma)/2$ both the large and small-field oscillations fully penetrate the sample. For $Z>D(1-2/\gamma)/2$ only the large-field oscillation fully penetrates the sample. Hence there are three types of Bean profiles to consider. The first is related to the low-field Bean profiles of Fig. 2, where neither field oscillation penetrates the sample. The second type of Bean profiles are described in

TABLE I. Summary of harmonic voltages calculated for different experimental configurations. A sample that oscillates in a constant field gradient and one that oscillates symmetrically about a ''flat roof'' field profile are considered. The star (*) notes that these harmonic frequencies can appear if a small sample (smaller than the throw distance of the V.S.M.) oscillates non-symmetrically about the peak in the applied field.

Experimental configuration	Even Multiple of Drive Frequency	Odd Multiples of Drive Frequency
Sample oscillation in a constant field gradient and centered in the pick-up coils ($\beta_0 \neq 0$, $\beta_1 = 0$)	2f, 4f, 6f, ...	1f only
Sample oscillating in a constant field gradient. Contribution from the sample not centered in the pick-up coils ($\beta_0 = 0$, $\beta_1 \neq 0$)	None	1f, 3f, 5f, ...
Sample centered in the dc applied field and centered in the pick-up coils ($\beta_0 \neq 0$, $\beta_1 = 0$)	None*	1f, 3f, 5f, ...
Sample centered in the dc applied field. Contribution from the sample not centered in the pick-up coils. ($\beta_0 = 0$, $\beta_1 \neq 0$)	2f, 4f, 6f, ...	None*

Fig. 9 for Z^* positive, where only the large-field oscillation penetrates the sample. The parameters which must be included in the calculation are t_c, which is the time when the point of the sample under consideration crosses the field center and t_{pa} and t_{pb}, which are the times when the field profile of the sample is completely reversed by the large field oscillation. The third type of profiles consider when both the large and the small oscillation fully penetrate the sample. The magnetic moment of each element in the central region was calculated over the relevant time intervals and integrated for $-D/2 < Z^* < D/2$ to give the total magnetic moment of the sample. Once the time dependence of the magnetic moment was calculated as a function of field, the instantaneous voltage and its Fourier component loss and lossless voltages were calculated following the procedure used in Sec. II B.

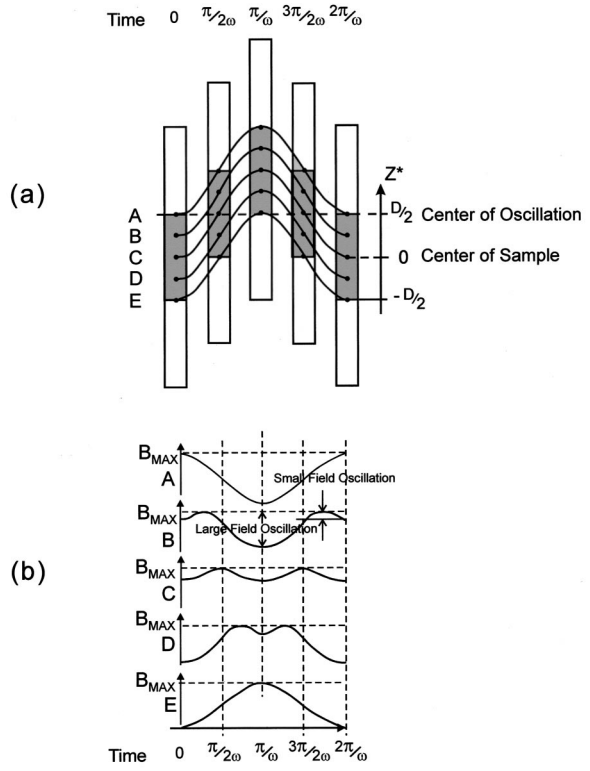

FIG. 7. The field experienced by a sample oscillating about the center of the applied field. (a) The movement of the sample from time $t=0$ to $t=2\pi/\omega$. The center of the oscillation is fixed. The parameter Z^* describes the position of an element of the sample with respect to the center of the sample. (b) The instantaneous field for points within the sample marked *A* to *E*.

In Fig. 10, the voltages generated at the even harmonic voltages for the positive half of the central region (i.e., $Z^* > 0$) are shown. These results apply for a small sample (smaller than the throw distance of the VSM) that oscillates nonsymmetrically about the peak in the applied field. However the Z^* positive and Z^* negative sections of the central region described in Fig. 7 produce equal and opposite even harmonic voltages and equal odd harmonic voltages. Hence the total signal for the entire central region only produces voltages at odd harmonics of the drive frequency. The odd harmonics for the central region are shown in Fig. 11. Calculations were completed for increasing and decreasing ap-

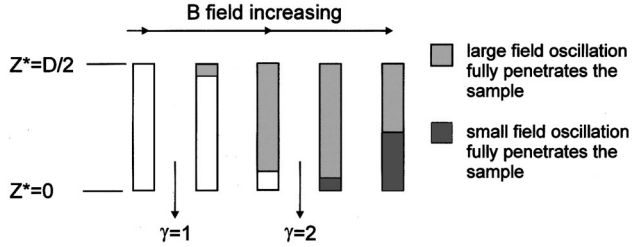

FIG. 8. A schematic showing how full penetration develops as the applied field increases for the upper part of the region of the sample (i.e., $0 < Z^* < D/2$) that sweeps through the peak in the applied field.

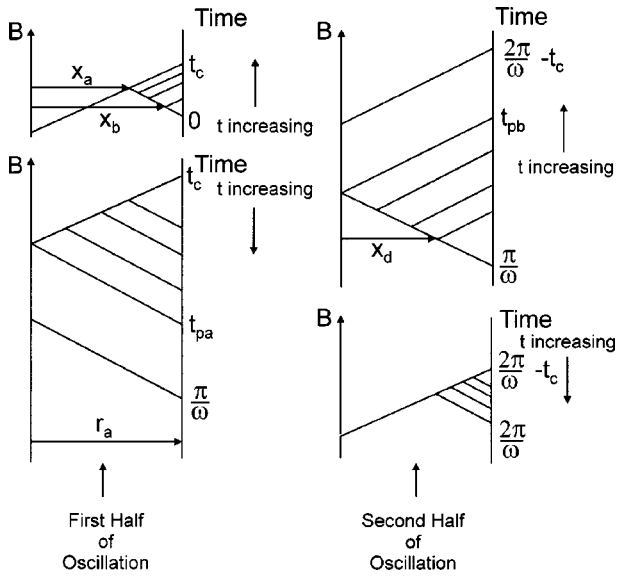

FIG. 9. The Bean profiles that occur in the intermediate field regime (i.e., $1<\gamma<2$) for the upper part of the region of the sample (i.e., $0<Z^*<D/2$) that sweeps through the peak in the applied field. t_c is the time when the point of the sample under consideration crosses the field center and t_{pa} and t_{pb} are the times when the field profile is completely reversed by the large field oscillation.

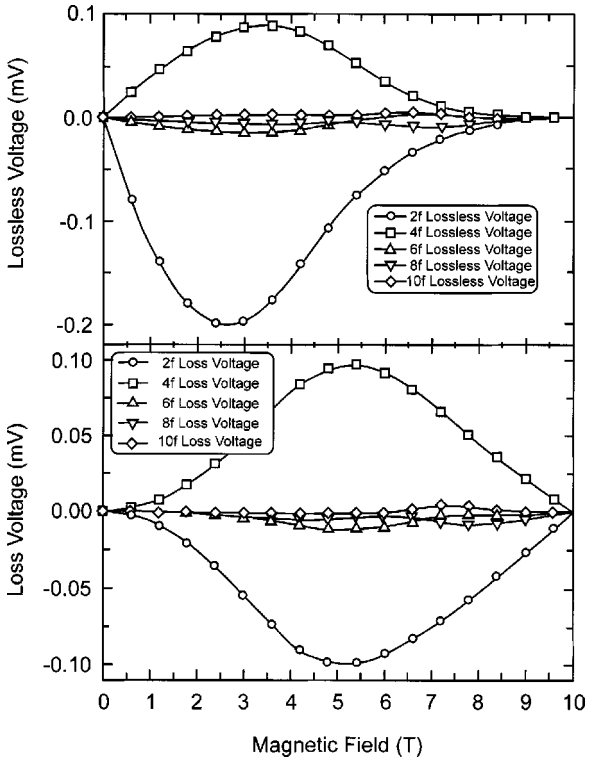

FIG. 10. Calculated values of the even harmonic voltages for the upper part of the region of the sample (i.e., $0<Z^*<D/2$) that sweeps through the peak in the applied field. The lower part of the sample (i.e., $0<Z^*<-D/2$) gives equal and opposite voltage so that a sample that oscillates symmetrically about the field center gives net zero even harmonic voltages. The sample is characterized by $J_C=5\times10^5(B_{C2}-B)\ \mathrm{A.m^{-2}}$, $B_{C2}=10\ \mathrm{T}$ and $l=10^{-3}\ \mathrm{m}$ and $r_m=10^{-3}\ \mathrm{m}$.

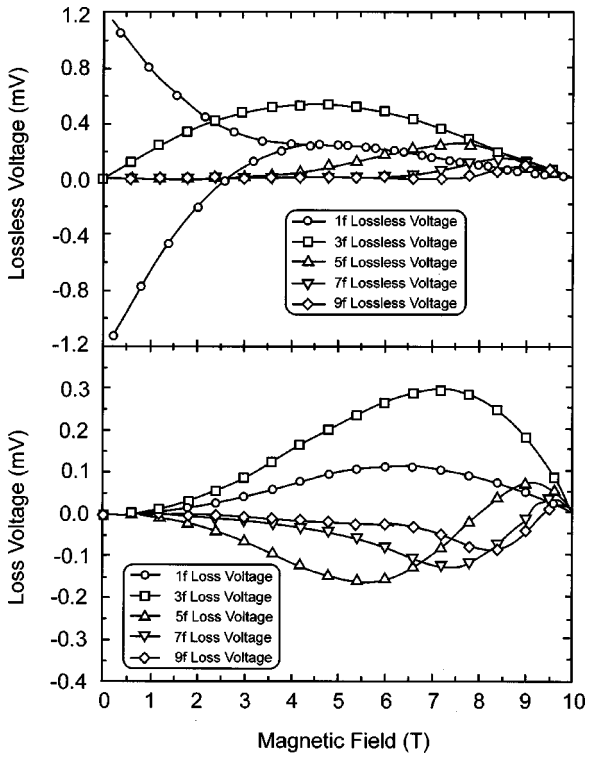

FIG. 11. Calculated odd harmonic voltages as a function of dc magnetic field for the section of a sample that crosses the field center perfectly centered within the magnet and the pick-up coils. Upper panel—lossless voltages. Note the paramagnetic reversible contribution in the 1f component. Lower panel—loss voltages. The sample is characterized by $J_C=5\times10^5(B_{C2}-B)\ \mathrm{Am^{-2}}$, $B_{C2}=10\ \mathrm{T}$, $l=10^{-3}\ \mathrm{m}$ and $r_m=10^{-3}\ \mathrm{m}$. The upper and lower parts of the sample produce even harmonic voltages that cancel to give zero.

plied field, with hysteresis only found in the 1f lossless voltage. The voltage measured at the drive frequency (i.e., 1f lossless voltage) contains both an irreversible component until $\gamma=2$ and a strictly reversible component at higher fields up to B_{C2}. The hysteresis of the 1f lossless voltage collapses to zero when $\gamma(=FB/\mu_0 J_C r_m)=2$ rather than $\gamma=1$ since the change in field experienced by this sample at the center is half of that when it does not cross the turning point in the dc field. Figure 11 demonstrates that even when the sample is properly centered both in the pick-up coils and the magnet, above B_{IRR} there is a 1f voltage, which contributes a reversible paramagnetic contribution and (similar to the harmonics) is nonzero up to B_{C2}. Because of the importance of this result, the reversible component is confirmed to be paramagnetic rather than diamagnetic as follows: Using Eq. (2), it can been seen that if the magnetic moment is constant (M_c) and paramagnetic, the voltage (V_c) across the coils is given by $V_c=G\beta_0\omega M_c \sin\omega t$, so that the coefficient of the lossless component is positive. Consider a sample oscillating about the center of the field and pick-up coils when $\gamma=2$. At the positions when it is instantaneously stationary during the cycle the magnetic moment will be at its maximum value and positive since the sample's immediate history will be that of decreasing magnetic field. Equally at the center of its oscillation the instantaneous magnetic moment will be at its maximum negative value. Hence, to first order the magnetic moment will be of the form $M_1\cos 2\omega t$ where M_1 is posi-

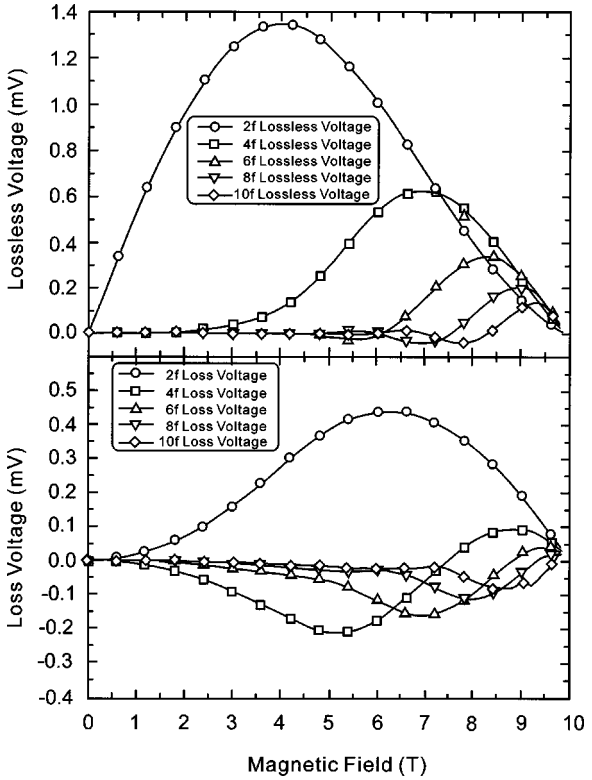

FIG. 12. Calculated additional harmonic voltages as a function of dc magnetic field due to the sample not centered in the pick-up coils (i.e., $\beta_1=-2$) but oscillating about the peak field. Upper panel—lossless voltages. Lower panel—loss voltages. All the even harmonic voltages tend to zero at B_{C2}. The sample is characterized by $J_C=5\times10^5(B_{C2}-B)$ Am^{-2}, $B_{C2}=10$ T and $l=4\times10^{-3}$ m and $r_m=10^{-3}$ m.

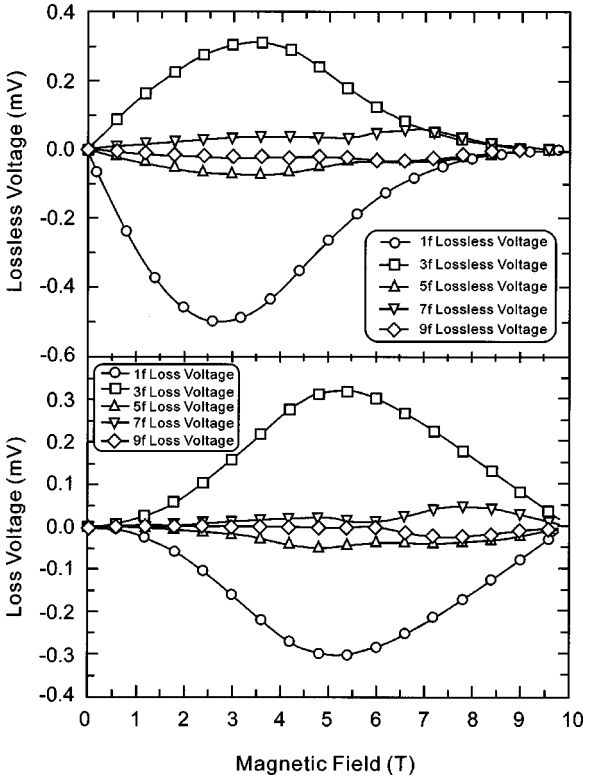

FIG. 13. Calculated additional harmonic voltages as a function of dc magnetic field for the upper part of the region of the sample not centered in the pick-up coils (i.e., $\beta_1=-2$) but sweeping through the peak field. Upper panel—lossless voltages. Lower panel—loss voltages. All the odd harmonic voltages tend to zero at B_{C2}. The lower part of the sample (i.e., $0<Z^*<-D/2$) gives equal and opposite voltage so that a sample that oscillates symmetrically about the field center gives net zero odd harmonic voltages. The sample is characterized by $J_C=5\times10^5(B_{C2}-B)$ Am^{-2}, $B_{C2}=10$ T and $l=10^{-3}$ m and $r_m=10^{-3}$ m.

tive. Using Eq. (2) and the vector identity $\cos 2\omega t\cos\omega t=1/2(\cos\omega t+\cos 3\omega t)$, the coefficient of the lossless component at the drive frequency is positive. Hence the reversible magnetic moment measured at $\gamma=2$, due to the nonzero J_C produces a paramagnetic contribution.

Finally consider the additional voltages produced by a sample off-centered in the pick-up coils oscillating about field center (i.e., $\beta_0=0$ and $\beta_l=-2$). The even voltages are shown in Fig. 12 and the odd voltages for positive section of the sample (i.e., $Z^*>0$) in Fig. 13. The odd voltages were equal and opposite in the two halves of the sample and hence sum to zero for the entire sample. The even voltages are the same for the two halves of the sample and hence have a nonzero sum.

Table I includes a summary of the results for a sample oscillating about the field center. The third row of data shows that only odd harmonics are generated for a sample properly centered in the magnet and in the pick-up coils. The 1f harmonic has both a hysteretic and a reversible component up to $\gamma=2$. Above $\gamma=2$, there is only a reversible paramagnetic signal. If the sample is centered in the magnet but not in the pick-up coils, there is an additional signal at all even harmonics (c.f. the bottom row of data). The sign of these signals is dependent on whether the sample is above or below the center of the pick-up coils.

D. The effect of the field dependence of J_C

The generality of the results obtained has been confirmed by repeating the calculations using different field dependencies for J_C and different values of superconducting parameters, sample sizes and field inhomogeneities.[30] Figures 14–16 are a sample of these calculations. A Kramer dependence for J_C has been considered of the form.[31]

$$J_C=\frac{\alpha}{B^{1/2}}(B_{C2}-B)^2, \tag{6}$$

where B_{C2} is the upper critical field and α is 5×10^5 Am^{-2} T$^{-3/2}$. In Fig. 14, the loss and lossless voltages for a sample that sees a constant field gradient (i.e., doesn't cross the magnet field center) but is properly centered in the pick up coils is shown. This figure is equivalent to Fig. 5. In Fig. 15, the harmonic voltages generated by a sample perfectly centered in the pick-up coils and the magnet are shown. The hysteretic 1f voltage collapses at $\gamma=2$ as found in Fig. 11 and a reversible paramagnetic voltage is found above B_{IRR}. Figure 16 shows how changing B_{C2} in Eq. (6) affects the results. The apparent J_C taken from the hysteresis of the 1f voltage drops to zero at fields far below B_{C2}, equivalent to when $\gamma=2$.

III. EXPERIMENTAL RESULTS

Experiments have been performed to test the calculations above, using a VSM developed in-house. It operates inside

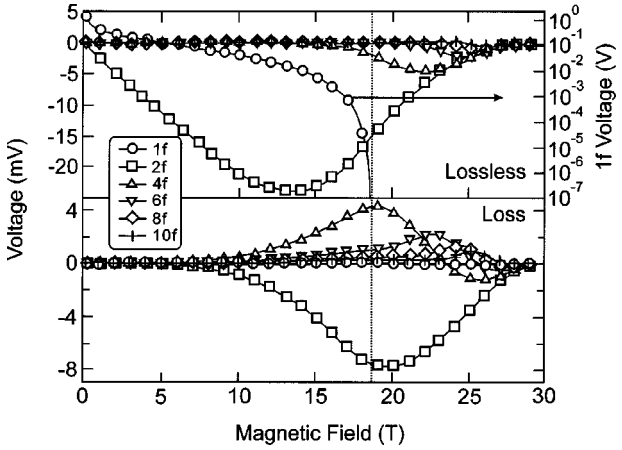

FIG. 14. Calculated harmonic voltages as a function of dc magnetic field for a sample in a uniform applied field gradient, centered in the pick-up coils. Upper panel left-hand axis—lossless voltages. All the odd harmonic voltages are zero except the fundamental frequency (1f), which alone changes sign (from diamagnetic shown when the dc field is increased) to paramagnetic when the dc field is decreased. All even harmonic voltages tend to zero at B_{C2}. Upper panel right-hand axis—the size of the hysteresis in the 1f voltage. Note the hysteresis drops to zero below 20 T although J_C is nonzero up to 30 T. Lower panel—loss voltages. All the odd harmonic voltages (including the fundamental that is shown) are zero. The dotted line indicates $\gamma=1$. The sample is characterized by $J_C=5\times10^5(B_{C2}-B)^2/B^{1/2}\,\mathrm{Am}^{-2}$, $B_{C2}=30\,\mathrm{T}$ and $l=4\times10^{-3}\,\mathrm{m}$ and $r_m=10^3\,\mathrm{m}$.

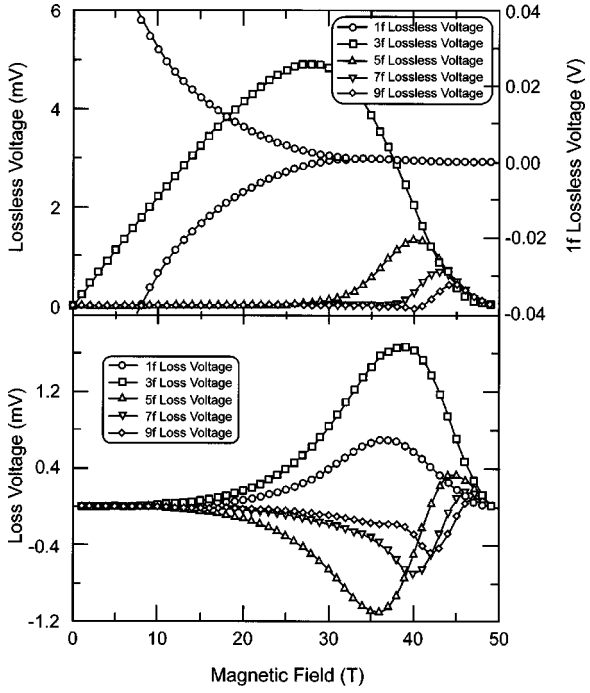

FIG. 15. Calculated harmonic voltages as a function of dc magnetic field for a sample in a uniform applied field gradient, centered in the pick-up coils. Upper panel—lossless voltages. All the even harmonic voltages are zero. Note that the hysteresis drops to zero below 30 T although J_C is nonzero. The 1 f signal scale is the right-hand axis. Lower panel—loss voltages. All the even harmonic voltages are zero. The sample is characterized by $J_C=5\times10^5(B_{C2}-B)/B^{1/2}\,\mathrm{Am}^{-2}$, $B_{C2}=50\,\mathrm{T}$ and $l=4\times10^{-3}\,\mathrm{m}$ and $r_m=10^{-3}\,\mathrm{m}$.

an Oxford Instruments 15 T, 40 mm bore solenoid magnet with a homogeneity over a 1 cm diameter spherical volume of 1 part in 10^3. Harmonics of the drive frequency up to 10f were measured as the field was swept from 0 to 15 T while the temperature was held constant. There were two experimental complexities. First the drive oscillation is not a pure sine wave at 1f. The oscillation includes a 7.5% 3f component. The 2f, 3f, 5f and 6f components occur at the 1–2 % level. Second, relatively large samples (compared to the throw distance) are required to obtain good signal to noise. A first-order correction was used to subtract the effect of the anharmonicity, which removed all hysteresis from the harmonics.

A sample of $SnMo_6S_8$ of dimensions 5.55 mm long and cross-sectional area 2.45 mm×1.88 mm was measured as a function of field at a temperature of 8.4 K. It was centered within the pick-up coils which were positioned 5 cm above the center of the dc field.[30] This configuration maximizes the even harmonic voltages (or equivalently magnetic moments). Odd frequency harmonics were observed, consistent with the sample not centered in the pick-up coils by ~0.5 mm. The data obtained at 1 f and the even harmonic magnetic moments are shown in Fig. 17. These data can be compared directly with Fig. 14. Good agreement is shown in both the relative magnitudes of the maxima and minima of the harmonics and in their position relative to B^*_{IRR}. For example, the turning points for the 2f- and 4f-lossless voltages occur at fields below and above B^*_{IRR} respectively, consistent with the upper panel in Fig. 14. Turning points for the 2f- and 4f-loss voltages occur just above B^*_{IRR} consistent with the lower panel in Fig. 14. The nonzero values for the harmonics above 7 T in Fig. 17 demonstrate explicitly that $J_C\neq0$ at B^*_{IRR}. Indeed the higher harmonic measurements demonstrate that J_C is not below the detection limit of the instrument until above 10 T—more than 3 T above B^*_{IRR}. Hence by measuring the harmonic voltages, one can determine whether J_C is zero (or more strictly, below the detection limit) at B^*_{IRR}. We have also measured $PbMo_6S_8$ and NbTi and confirmed that the agreement between data and the calculations is not de-

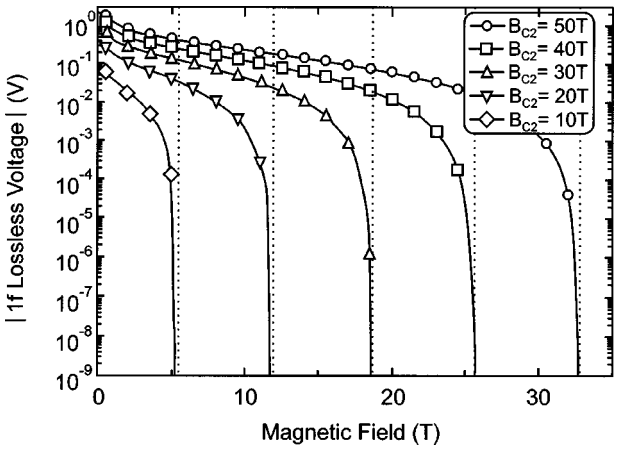

FIG. 16. The magnitude of the hysteresis in the 1f lossless voltage for different values of upper critical field. The current density of the sample follows Kramer's law where $J_C=5\times10^5(B_{C2}-B)^2/B^{1/2}\,\mathrm{Am}^{-2}$.

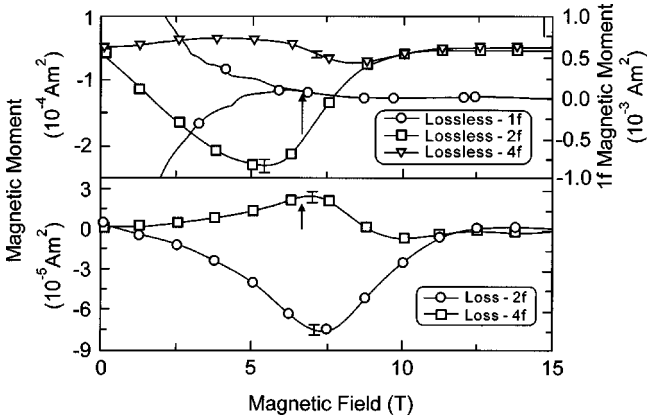

FIG. 17. Harmonic measurements on a $SnMo_6S_8$ sample as a function of applied dc field at 8.4 K. The sample is centered in the pick up coils, +5 cm above the dc field center. The arrows indicate $\gamma=1$. The sample oscillates in a constant field gradient.

pendent on the superconducting material.[30]

In order to further investigate the effect of field inhomogeneity on $B^*_{\rm IRR}$, the pick-up coils were displaced from the center of the magnet by +2 cm and +5 cm and the sample centered in the pick-up coils. The 1f lossless magnetic moment for the $SnMo_6S_8$ sample was measured as a function of field gradient and temperature to investigate the effect of ac field on the critical current density and irreversibility field. The results are shown in Fig. 18 where the dotted lines (a) to (d) represent $\gamma=1$ for the 8.4 K+5 cm, 8.4 K+2 cm, 6.8 K +5 cm and 6.8 K+2 cm measurements respectively. γ is calculated by using the field-center measurement as giving a first-order value for the actual critical current density and the measured inhomogeneity of the magnet. The dotted lines correlate very well with the measured irreversibility field. We conclude that although at each temperature, the measured critical current values (derived from the hysteresis using Bean's model) drop rather rapidly at the highest fields, the field values at which the measured critical current density drops to zero gives values for $B^*_{\rm IRR}$ not $B_{\rm IRR}$. The data in Fig. 17 at 8.4 K clearly show a harmonic signal above 10 T, which is not seen in the 1f data of Fig. 18.

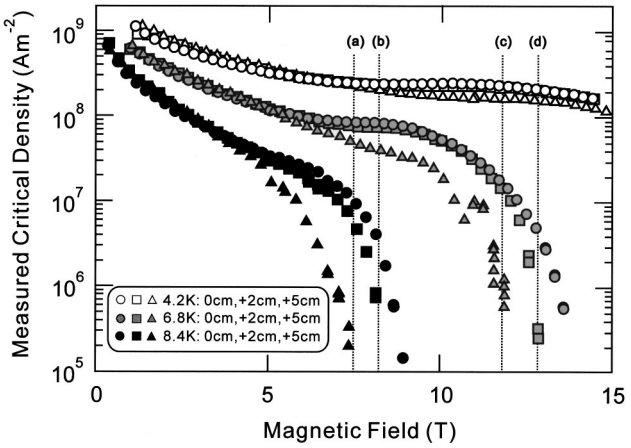

FIG. 18. The measured critical current density derived from Bean's critical-state model for $SnMo_6S_8$ as a function of applied dc field and temperature. The dotted lines represent $\gamma=1$ for (a) the sample at 8.4 K and displaced from the peak in the dc field by +5 cm, (b) 8.4 K, 2 cm, (c) 6.8 K, 5 cm and (d) 6.8 K, 2 cm.

IV. DISCUSSION

A. The magnetic phase diagram of superconductors

In single phase, highly ordered low-temperature superconductors such as Nb or Nb_3Sn, the temperature dependence of the lower and upper critical fields characterize quite comprehensively the magnetic phase diagram. After the discovery of the high-temperature superconductors, it has become clear that many other critical parameters and processes are important throughout much of the magnetic phase diagram including the melting temperature (T_M) where the order in the flux-line-lattice changes discontinuously, fluctuation effects close to B_{C2}, thermally activated flux creep[32] and in highly anisotropic or layered HTS materials, a two-dimensional—three-dimensional crossover,[33] where the Abrikosov flux lines break down into quasi-two-dimensional so-called pancakes.[34] One of the important developments in the last few years has been clear specific heat,[35–37] neutron-scattering,[38] and magnetic[39] measurements of the melting line in very clean materials. Nevertheless the general relationship between $B_{\rm IRR}$ and T_M is still not known. In very clean $YBa_2Cu_3O_1$, it has been suggested that T_M and $B_{\rm IRR}$ have a common origin.[40] In $Bi_2Sr_2Ca_1Cu_2O_8$, when bulk pinning has been eliminated, $B_{\rm IRR}$ and T_M are not related.[41,42]

In addition to the magnetic measurements of $B_{\rm IRR}$ there are complementary transport measurements which follow well-established scaling laws[43] for both low[44] and high[45] temperature superconductors. However, although these scaling laws give clear signatures for when J_C drops to zero, they can equally describe systems that cross-over from percolative to nonpercolative properties. Hence the interpretation of the parameters derived from resistive data can equally be in terms of giving the boundary for zero-resistance percolation in a highly disordered or inhomogeneous superconductor[46] or in terms of a transition from a pinned to unpinned vortex liquid.[47,48] To contribute to unravelling the complexity of magnetic phase diagrams, we suggest that measurements of $B_{\rm IRR}$ and κ can be improved to give data closer to the ultimate sensitivity of the instrument rather than limited by the field inhomogeneity of the magnet.

B. Increasing J_C, $B_{\rm IRR}$ and $B^*_{\rm IRR}$

The marked effect of field inhomogeneity on SQUID measurements has broadly been overcome by significantly improving the homogeneity of the magnets used. Nevertheless it is clear that inevitably the self-field of the sample will eventually be sufficiently small to equal the variation in field seen during the movement of the sample during the SQUID measurement. At this point, the sample will be fully penetrated, the magnetic hysteresis will be washed out and as noted above $B^*_{\rm IRR}$ is measured rather than $B_{\rm IRR}$. Hence the origin of $B^*_{\rm IRR}$ is similar in a VSM and a SQUID measurement. Flux pinning scaling laws in low-temperature superconductors show that J_C scales with B^n_{C2} where n is typically 2 to 3.[49,50] When materials have an irreversibility field significantly below B_{C2}, $B_{\rm IRR}$ becomes the natural field scale for the scaling laws. One may then expect that as the $B_{\rm IRR}$ in-

creases, J_C increases. There have been a number of reports that radiation increases both the irreversibility line and J_C in both $YBa_2Cu_3O_7$ (Ref. 51) and $Bi_2Sr_2Ca_2Cu_3O_{10}$.[52] However this article has shown that for a given magnetic instrument, one expects B^*_{IRR} to increase as J_C increases. Equally, measurements to test for granularity by taking large samples and grinding them into powder inevitably produce changes in B^*_{IRR} simply because of the change in the dimensions of the sample. Measurements on small samples such as single crystals are prone to error because of the small self-field produced by such samples. Measurements of κ, particularly those that show curvature in the reversible magnetization data[11] may include a contribution from non-zero J_C. The general concerns arise whether reports in the literature of reversible magnetization data can correctly be equated to theoretical thermodynamic calculations of the diamagnetic response of superconductors and furthermore whether reports of B_{IRR} are in fact reports of B^*_{IRR}. We have shown experimentally that these parameters can differ in high fields by many T.

C. Measuring κ, J_C, and B_{IRR}

The calculations presented are sufficiently wide-ranging to allow the qualitative harmonic response of a range of different sample sizes and geometries to be determined—samples that are much bigger or much smaller than the throw distance, or that are symmetrically oscillating about the magnetic field center or not, or that are centered in the pick-up coils or not.

The basic difference in the solutions in Sec. II B and II C can be utilized to improve measurements of κ, J_C and B_{IRR}. Consider a sample in a magnetic field above B^*_{IRR} that is centered in the pick-up coils. If the sample sees a constant field gradient across the throw distance the magnetic moment changes sign twice during the cycle and the 1 f signal is zero (c.f., Fig. 5). If the sample oscillates about the field center, the magnetic moment changes sign four times and a reversible magnetic component is produced (c.f. Figs 11 and 13). We propose that if preliminary calculations show that the field inhomogeneity in the magnetic instrument may produce significant errors for a sample of interest, a reasonable first step would be to slightly offset the pick-up coils and the sample so that the sample does not cross the field center during its oscillation and remeasure it. If the data changes significantly, we propose that the system is recentered and that an additional coil system is added to the instrument to produce a field gradient sufficiently large to ensure the magnetic moment only changes sign twice during a single oscillation. For a sample perfectly centered in the pick-up coils, this additional field gradient will significantly reduce any contribution at 1 f from non-zero J_C above B^*_{IRR} (c.f., Fig. 5). We propose that two sets of reversible magnetization data are obtained with the gradient field in opposite directions. The average of these data sets will cancel to first order the effect of the sample not being centered in the pick-up coils perfectly (c.f., Fig. 6). From these reversible magnetization data obtained at the drive frequency of the VSM, more reliable measurements of κ can be made than would be possible using standard methods. If two sets of measurements are also made at higher harmonics, the reversible voltages due to any noncentering of the sample in the pick-up coils are again cancelled to first order and the entire voltage signal can be reconstructed from the harmonic data. Equation (2) can then be used to deconvolute the time dependence of the magnetic moment from which J_C can be extracted. Once J_C has been accurately measured, an accurate measurement of B_{IRR} is then available.

V. CONCLUSIONS

The magnetic phase diagram of superconductors has been much debated, particularly with respect to high-temperature superconductors. Many explanations have been proposed for the region of phase space that appears to have no pinning, yet is still superconducting. VSM measurements are commonly used in high magnetic fields to determine the phase boundary when J_C is zero.[20] However, B^*_{IRR} is determined by sample geometry, field inhomogeneity and throw distance, and cannot be equated to B_{IRR}. When the sample is centered in both the magnetic field and the VSM pick-up coils, the reversible signal at the drive frequency in high fields includes two contributions. In addition to the usual diamagnetic contribution from the thermodynamic reversible magnetization of the superconductor, there is a reversible paramagnetic contribution from the nonzero J_C. Hence above B^*_{IRR}, the reversible magnetization cannot be equated to the thermodynamic reversible magnetization, and hence κ cannot be reliably derived, unless it is shown that J_C is negligible. We have proposed a method to improve measurements of κ, J_C and B_{IRR} by adding a coil system to the instrument that produces a constant field gradient over the throw distance of the sample. Harmonics measurements are proposed to improve the accuracy of J_C and B_{IRR} data. Experimental data have been presented to support the conclusions of this work.

ACKNOWLEDGMENTS

The authors thank the E.P.S.R.C. and Oxford Instruments Plc for providing support for this work and R. Luscombe, K. Brazier, D. N. Zheng, and N. Cheggour for helpful discussions.

[1] E. H. Brandt, Int. J. Mod. Phys. B **5**, 751 (1991).
[2] G. Blatter, M. V. Feigelman, V. B. Geshkenbein, A. I. Larkin, and V. M. Vinokur, Rev. Mod. Phys. **66**, 1125 (1994).
[3] Y. Yeshurun, A. P. Malozemoff, and A. Shaulov, Rev. Mod. Phys. **68**, 911 (1996).
[4] L. F. J. Cohen and H. J. Jensen, Rep. Prog. Phys. **60**, 1581 (1997).
[5] M. K. Wu, J. R. Ashburn, C. J. Torng, P. H. Hor, R. L. Meng, L. Gao, Z. J. Huang, Y. Q. Wang, and C. W. Chu, Phys. Rev. Lett. **58**, 908 (1987).
[6] M. Suenaga, G. Ghosh, Y. Xu, and D. O. Welch, Phys. Rev. Lett.

66, 1777 (1991).
[7] D. N. Zheng, H. D. Ramsbottom, and D. P. Hampshire, Phys. Rev. B **52**, 1 (1995).
[8] D. N. Zheng, A. M. Campbell, and R. S. Liu, Phys. Rev. B **48**, 6519 (1993).
[9] J. Y. Genoud, G. Triscone, A. Junod, T. Tsukamoto, and J. Muller, Physica C **242**, 143 (1995).
[10] V. L. Ginzburg and L. D. Landau, Zh. Eksp. Teor. Fiz. **20**, 1064 (1950).
[11] Z. Hao, J. R. Clem, M. W. McElfresh, L. Civale, A. P. Malozemoff, and F. Holtzberg, Phys. Rev. B **43**, 2844 (1991).
[12] S. Foner, Rev. Sci. Instrum. **30**, 548 (1959).
[13] S. Libbrecht, E. Osquiguil, and Y. Bruynseraede, Physica C **225**, 337 (1994).
[14] G. Ravikumar *et al.*, Physica C **276**, 9 (1997).
[15] A. Schilling, H. R. Ott, and T. Wolf, Phys. Rev. B **46**, 14 253 (1992).
[16] L. Pust, D. Dlought, and M. Jirsa, Supercond. Sci. Technol. **9**, 814 (1996).
[17] I. Hlasnik, M. Majoros, and L. Jansak, *Handbook of Applied Superconductivity* (Institute of Physics, Bristol, 1998).
[18] A. Zieba and S. Foner, Rev. Sci. Instrum. **53**, 1344 (1982).
[19] C. P. Bean, Rev. Mod. Phys. **36**, 31 (1964).
[20] J. R. Cave, *Handbook of Applied Superconductivity* (Ref. 17).
[21] J. Mallinson, J. Appl. Phys. **37**, 2514 (1966).
[22] A. M. Campbell, J. Phys. C **2**, 1492 (1969).
[23] A. M. Campbell and J. E. Evetts, Adv. Phys. **21**, 199 (1972).
[24] H. D. Ramsbottom and D. P. Hampshire, J. Appl. Phys. **85**, 3732 (1999).
[25] L. Ji, R. H. Sohn, G. C. Spalding, C. J. Lobb, and M. Tinkham, Phys. Rev. B **40**, 10 936 (1989).
[26] S. K. Ghatak, A. Mitra, and D. Sen, Phys. Rev. B **45**, 951 (1992).
[27] R. B. Goldfarb, A. F. Clark, A. I. Braginski, and A. J. Panson, Cryogenics **27**, 475 (1987).
[28] C. P. Bean, Phys. Rev. Lett. **8**, 250 (1962).
[29] R. G. Hampshire and M. T. Taylor, J. Phys. F: Met. Phys. **2**, 89 (1972).
[30] I. J. Daniel, Ph.D. thesis, Durham University, 1999.
[31] E. J. Kramer, J. Appl. Phys. **44**, 1360 (1977).
[32] Y. Yeshurun and A. P. Malozemoff, Phys. Rev. Lett. **60**, 2202 (1988).
[33] L. I. Glazman and A. E. Koshelev, Phys. Rev. B **43**, 2835 (1991).
[34] J. R. Clem, Phys. Rev. B **43**, 7837 (1991).
[35] M. Roulin, A. Junod, and E. Walker, Science **273**, 1210 (1996).
[36] M. Roulin, A. Junod, A. Erb, and E. Walker, Phys. Rev. Lett. **80**, 1722 (1998).
[37] B. Revaz, A. Junod, and A. Erb, Phys. Rev. B **58**, 11 153 (1998).
[38] R. Cubitt *et al.*, Nature (London) **365**, 407 (1993).
[39] B. Revaz, G. Triscone, L. Fabrega, A. Junod, and J. Muller, Europhys. Lett. **33**, 701 (1996).
[40] J. R. Cooper, J. W. Loram, J. D. Johnson, J. W. Hodby, and C. Changkang, Phys. Rev. Lett. **79**, 1730 (1997).
[41] E. Zeldov, D. Majer, M. Konczykowski, V. B. Geshkenbein, V. M. Vinokur, and H. Shtrikman, Nature (London) **375**, 373 (1995).
[42] D. Majer, E. Zeldov, and M. Konczykowski, Phys. Rev. Lett. **75**, 1166 (1995).
[43] R. H. Koch, V. Foglietti, W. J. Gallagher, G. Koren, A. Gupta, and M. P. A. Fisher, Phys. Rev. Lett. **63**, 1511 (1989).
[44] N. Cheggour and D. P. Hampshire, in *Applied Superconductivity 1997*, edited by H. Rogalla and D. H. A. Blank, IOP Conf. Proc. No. 158 (Institute of Physics, London, 1997), p. 1275.
[45] K. Yamafuji and T. Kiss, Physica C **290**, 9 (1997).
[46] D. C. Harris, S. T. Herbert, D. Stroud, and J. C. Garland, Phys. Rev. Lett. **67**, 3606 (1991).
[47] R. Prozorov, M. Konczykowski, B. Schmidt, Y. Yeshurun, A. Shaulov, C. Villard, and G. Koren, Phys. Rev. B **54**, 15 530 (1996).
[48] M. V. Indenbom, C. J. vander Beek, V. Berseth, M. Konczykowski, N. Motohira, H. Berger, and W. Benoit, J. Low Temp. Phys. **105**, 1117 (1996).
[49] W. A. Fietz and W. W. Webb, Phys. Rev. **178**, 657 (1969).
[50] D. Dew-Hughes, Philos. Mag. **30**, 293 (1974).
[51] L. Civale, A. D. Marwick, T. K. Worthington, M. A. Kirk, J. R. Thompson, L. Krusin-Elbaum, Y. Sun, J. R. Clem, and F. Holtzberg, Phys. Rev. Lett. **67**, 648 (1991).
[52] Q. Li, Y. Fukumoto, Y. Zhu, M. Suenaga, T. Kaneko, K. Sato, and C. Simon, Phys. Rev. B **54**, R788 (1996).